arXiv:1401.1650v1 [cond-mat.mtrl-sci] 8 Jan 2014

Li dynamics in carbon-rich polymer-derived SiCN ceramics probed by NMR

Seung-Ho Baek[a,*], Lukas Mirko Reinold[b], Magdalena Graczyk-Zajac[b], Ralf Riedel[b], Franziska Hammerath[a], Bernd Büchner[a,c], Hans-Joachim Grafe[a]

[a] *IFW-Dresden, Institute for Solid State Research, PF 270116, 01171 Dresden, Germany*
[b] *Technische Universität Darmstadt, Fachbereich Material- und Geowissenschaften, Fachgebiet Disperse Feststoffe, Jovanka-Bontschits-Straße 2, 64287 Darmstadt, Germany*
[c] *Institut für Festkörperphysik, Technische Universität Dresden, 01062 Dresden, Germany*

Abstract

We report ^{7}Li, ^{29}Si, and ^{13}C NMR studies of two different carbon-rich SiCN ceramics SiCN-1 and SiCN-3 derived from the preceramic polymers polyphenylvinylsilylcarbodiimide and polyphenylvinylsilazane, respectively. From the spectral analysis of the three nuclei at room temperature, we find that only the ^{13}C spectrum is strongly influenced by Li insertion/extraction, suggesting that carbon phases are the major electrochemically active sites for Li storage. Temperature (T) and Larmor frequency (ω_L) dependences of the ^{7}Li linewidth and spin-lattice relaxation rates T_1^{-1} are described by an activated law with the activation energy E_A of 0.31 eV and the correlation time τ_0 in the high temperature limit of 1.3 ps. The 3/2 power law dependence of T_1^{-1} on ω_L which deviates from the standard Bloembergen, Purcell, and Pound (BPP) model implies that the Li motion on the μs timescale is governed by continuum diffusion mechanism rather than jump diffusion. On the other

*Corresponding author. Tel:+49 (0)351 4659 801; fax: +49 (0)351 4659 313
Email address: sbaek.fu@gmail.com (Seung-Ho Baek)

hand, the rotating frame relaxation rate $T_{1\rho}^{-1}$ results suggest that the slow motion of Li on the ms timescale may be affected by complex diffusion and/or non-diffusion processes.

Keywords: Nuclear Magnetic Resonance (NMR), ^{7}Li dynamics, Anode, Lithium-ion battery, Silicon carbonitride, Polymer-derived ceramic

1. Introduction

Polymer-derived ceramics (PDCs) that consist of Si, C, O, and N possess novel physical, chemical, and mechanical features which can be tuned by subtle changes of composition and/or microstructure as well as of processing conditions, finding applications in a variety of fields such as fibers, brakes for vehicles, sealants, coatings, and sensors [1, 2].

Among the Si-based PDCs, SiCN and SiOC are promising candidates for anodes for Li-ion batteries to replace graphite anodes. They possess a high discharge capacity compared to that of graphite, thermal and chemical stability against corrosion, and cyclic stability during charge/discharge due to stable 3D network structure with amorphous nature [3, 4, 5, 6, 7, 8]. Recent studies were focused on the carbon-rich SiCN ceramics due to their increased thermal stability and electrochemical performance that are attributed to the free carbon phase imbedded into their microstructure [9, 10, 11, 12, 13].

While most of these studies concentrated on the static properties of these materials, such as electrochemical performance, discharge capacity, and the relation between microstructure and precursor polymer structure, it is also very important to understand the Li ion dynamics on various timescales, characterizing the Li mobility and diffusion mechanism, and to get informa-

tion on the storage site of the Li.

Nuclear magnetic resonance (NMR) has proven to be a powerful method for probing local structure and Li motions in numerous Li-containing ion conductors [14, 15, 16]. Although there have been a couple of solid state NMR studies performed on the SiCN and SiOC ceramics [17, 18, 19, 13], they are mostly concerned with structural aspects of these materials using the magic-angle spinning (MAS) technique, still lacking information on the Li dynamics as a function of temperature and frequency.

In this paper, we report ^{7}Li, ^{29}Si, and ^{13}C NMR studies of carbon-rich SiCN PDCs, adopting wide-line NMR method instead of its high-resolution solid state counterpart, providing information on the Li dynamics as well as on the Li storage site. While our data show that inserted Li ions mainly find carbons for their electrochemical storage sites, they also suggest that the mixed bond tetrahedra of Si which are formed in polysilazane-derived SiCN, act as an additional lithiation site. The spin-lattice relaxation rates as a function of temperature and frequency demonstrate that the Li motion on a timescale of μs is precisely described by an activated law $\tau_c = \tau_0 \exp(E_A/k_B T)$.

2. Sample preparation and experimental details

Two SiCN ceramics derived from polysilylcarbodiimide (HN1) and polysilazane (HN3) (in the following denoted by SiCN-1 and SiCN-3, respectively) have been synthesized, as described in detail in Refs. [13, 20]. The elemental composition of the ceramics with regard to their carbon, nitrogen, oxygen, chlorine and hydrogen content was measured. The carbon amount was de-

termined by a combustion analysis with a carbon analyzer Leco C-200, the nitrogen and oxygen content by hot gas extraction with a Leco TC-436 N/O analyzer (Leco Corporation, Michigan, USA). The chlorine and the hydrogen content were measured at the Mikroanalytisches Labor Pascher (Remagen, Germany). The silicon content was calculated as the difference of the above mentioned elements to 100 %.

The particle size distribution of the ceramic powders was measured with an analysette 22 COMPACT (Fritsch, Germany) which is working in a measurement range of 0.3 to 300 μm. The measurements were performed in ethanol at constant stirring and ultra sonic treatment. The specific surface area (SSA) and porosity of the samples were determined from the nitrogen adsorption and desorption isotherms with an Autosorb-3B (Quantachrome Instruments, USA) at 77 K using the Brunauer-Emmett-Teller equation and the Barret-Joyner-Halenda method, respectively.

The ceramic powders were mixed with 7.5 wt% of CarbonBlack Super P® (Timcal Ltd., Switzerland) and 7.5 wt% polyvinyilidenfluoride (PVDF, SOLEF, Germany) dissolved in N-methyl-2-pyrrolidone (NMP, BASF, Germany). The slurry was spread on a glass plate and dried at 40 °C for 24 h, scratched off and ground. Approximately 100 mg of the as prepared powder was pressed uniaxially with 30 kN for 5 min to obtain pellets with a diameter of 10 mm and a thickness of roughly 0.8 mm. The pellets were dried under vacuum in a Buchi® Glas Oven at 80 °C for 24 h and transferred into a glovebox (MBraun, Germany).

All together six samples have been prepared for NMR probing. One pellet of each ceramic was first fully lithiated and afterwards delithiated

following the later described procedure (in the following denoted as SiCN-1b and SiCN-3b). A second pellet of each ceramic was only fully lithiated (in the following denoted as SiCN-1a and SiCN-3a) and third pellet of each ceramic was prepared in the same manner as the above mentioned samples, however this samples was not tested electrochemically (in the following denoted as SiCN-1 as-prepared and SiCN-3 as-prepared).

Electrochemical testing was done in a two electrode Swagelok® type cell with lithium foil (99.9% purity, 0.75 mm thickness, Alfa Aesar, Germany) as counter/reference electrode, 1 M $LiPF_6$ in EC:DMC 1:1 wt% (LP30, Merck, Germany) as electrolyte and a glass fiber separator (QMA, Whatmann™, UK). Additionally a polypropylene separator (Celgard 2500, Celgard, USA) was placed between the glass fiber separator and the pellet to avoid contamination of the pellets with glass fibers. Lithiation and delithiation was performed with a VMP3 multipotentiostat (Biologic Science Instruments, France) at a current of 3.72 mA/g^{-1}, which is equivalent to a C-rate of C/100 in terms of the theoretical capacity of graphite. Measurements were performed at 25 °C and voltage limits were set to 0.005 V and 3 V vs. Li/Li^+. Afterwards the cells were disassembled in the glove box. The pellets were washed with DMC to remove the salt of the electrolyte and ground to a powder for NMR measurements.

The NMR measurements were performed using Tecmag Fourier Transform (FT) pulse spectrometer. ^{7}Li, ^{29}Si, and ^{13}C NMR spectra were obtained using a spin-echo pulse sequence ($\pi/2 - \tau - \pi$) which is more advantageous than the free induction decay (FID) method since it effectively eliminates spurious signals. For the ^{29}Si and ^{13}C, due to the weak signal intensity asso-

ciated with their low natural abundances and the long spin-lattice relaxation time T_1, their spectra were acquired only at room temperature for two phases (SiCN-1 as prepared and SiCN-1a) and three phases (SiCN-3 as prepared, SiCN-3a, and SiCN-3b). For these two nuclei, the NMR spectra each were averaged more than 4000 scans, with a typical $\pi/2$ pulse length of 4 μs and a repetition time of 40 s.

To probe the Li diffusion parameters, ^{7}Li NMR spectra and relaxation rates were measured as a function of temperature in the range of 80–420 K. The spin-lattice relaxation rates T_1^{-1} in the laboratory frame and $T_{1\rho}^{-1}$ in the rotating frame were measured to study the Li motions on μs and ms timescales, respectively. For the T_1^{-1} measurements, the saturation recovery method was employed and T_1 was obtained by fitting the relaxation of the nuclear magnetization $M(t)$ to a single exponential function, $1 - M(t)/M(\infty) = a\exp(-t/T_1)$ where a is a fitting parameter.

In this study, since SiCN-1 and SiCN-3 exhibit very similar electrochemical performance as well as NMR results at 116.64 MHz, the detailed frequency dependences of the linewidth and relaxation rates have been made only on SiCN-3a.

3. Experimental results and discussion

3.1. Characterization

The results of elemental composition are shown in Table 1. The table also includes the amount of free carbon within the ceramics calculated according to the equation,

$$\text{wt\%free C} = \frac{\left(x - 1 + \frac{y}{2} + \frac{3z}{4}\right) \cdot M_{\text{C}}}{M_{\text{Si}} + x \cdot M_{\text{C}} + y \cdot M_{\text{O}} + z \cdot M_{\text{N}}} \cdot 100 \qquad (1)$$

taken from Ref. [21] with x, y, z being taken from the empirical formula $SiC_xO_yN_z$ and M_C, M_{Si}, M_O and M_N being the molar mass of the corresponding elements. Both samples exhibit a high amount of free carbon and only little impurities of oxygen. The residual chlorine measured in the samples is due to end groups of chlorine at the synthesized polymers and leftovers of the byproduct trimethylchlorosilane of the synthesis reaction.

The evaluation of particle size distribution measurements lead to D_{50} values of 11.6 μm for SiCN-1 and 10.6 μm for SiCN-3, respectively. Both SiCN ceramics demonstrate a non-porous character with a SSA lower than 10 m^2g^{-1} and 15 m^2g^{-1} for SiCN-1 and SiCN-3, respectively.

3.2. Electrochemical results

Table 2 summarizes the lithiation and delithiation capacities of the investigated samples and the coulombic efficiency η of the samples SiCN-1b and SiCN-3b calculated as the ratio of delithiation capacity to lithiation capacity times 100. The corresponding voltage over capacity plots are shown in Fig. 1. Despite the low current applied for lithiation and delithiation, capacities for both materials are below the achieved capacities of printed electrodes. This discrepancy can be explained by the much higher thickness of the pellets needed for a suitable amount of powder for NMR probing.

3.3. NMR spectra at room temperature

Figures 2, 3, and 4 show the spin-echo spectra of ^{7}Li, ^{29}Si, and ^{13}C, respectively, acquired at room temperature in an external field of 7.0494 T (i.e. Larmor frequencies of 116.64 MHz, 59.624 MHz, and 75.476 MHz) for SiCN-1 and SiCN-3 samples.

The ^{7}Li spectra shown in Fig. 2 reveal a narrow linewidth of 2 kHz with a small positive shift for both SiCN-1a and SiCN-3a samples. In practice, we do not observe any noticeable difference between the ^{7}Li spectra of SiCN-1 and SiCN-3, suggesting that the Li dynamics is weakly sensitive to the precursor polymers. We also measured the ^{7}Li spectra in the discharged samples. Interestingly, we find that the Li ions associated with smaller shift largely remain after discharging for both samples. This finding suggests that it is more difficult to remove Li that occupies sites in isotropic surroundings with less chemical shifts.

Both samples SiCN-1 and SiCN-3 yield symmetric ^{29}Si spectra which are shown in Fig. 3 for the as-prepared and lithiated samples. It is interesting to note that for SiCN-3 the linewidth increases after charging and recovers that of the as-prepared after discharging, while there is no difference of the spectrum after charging for SiCN-1. This suggests that inserted Li ions are coupled to Si, leading to a larger distribution of the local field at the ^{29}Si, i.e. a larger linewidth, in SiCN-3. The fact that such a broadening does not occur in SiCN-1 implies that local structures of Si that may act as electrochemical Li storage sites are formed in the SiCN ceramic derived from HN3 but not from HN1.

While we observed a symmetric line for ^{29}Si, the ^{13}C spectrum is clearly resolved into two in the as-prepared SiCN sample, indicating the existence of two inequivalent carbon sites or environments as shown in Fig. 4. Since this carbon-rich SiCN ceramics contain a very high concentration of free carbon phases, we attribute these two peaks to the presence of sp^2 and sp^3 carbons [7, 20]. In fact, a previous high-resolution ^{13}C NMR study in SiCN

revealed two groups of spectra associated with sp^2 and sp^3 carbons [22]. They are roughly separated by $\sim$ 110 ppm, which indeed accounts for the difference between the main peak at $\sim$ 200 ppm and the shoulder at $\sim$ 90 ppm. Therefore, we assign the main peak and the shoulder to sp^2 and sp^3 carbons, respectively. This implies that the small amount of sp^3 carbons is still present even at the high pyrolysis temperature (1100 °C) in both SiCN-1 and SiCN-3.

The insertion of Li ions affects the ^{13}C spectrum significantly, reducing the anisotropy of the spectrum. This contrasts with the ^{29}Si spectrum which is almost intact with Li insertion for SiCN-1. The large influence of Li insertion on the ^{13}C spectrum indicates that electrochemically active sites for Li storage are mainly carbon phases. It would be interesting to recall a debate on the main Li storage in SiOC ceramics. Fukui et al. [18] suggested that the free carbon phase is the main site for Li storage, while Ahn et al. [21] proposed the mixed bond tetrahedra of Si as major Li hosting sites.

It is known that HN1-derived SiCN-1 has no concentration of mixed bonds of Si unlike HN3-derived SiCN-3 [4, 17]. Thus, based on the almost identical spectra of ^{13}C for both SiCN-1 and SiCN-3 samples after charging/discharging, one can argue that carbons are the major electrochemical storage site for the Li ions, regardless of the preceramic polymers. The fact that the whole ^{13}C spectrum, which reflects two inequivalent carbon phases, changes after charging/discharging in a reversible way implies that all carbon species participate in hosting Li ions and, once binding Li, both sp^2 and sp^3 carbons experience similar chemical environment surrounding them.

While the ^{13}C NMR results show the main role of free carbon phases as

the storage sites of Li, we note that the broadening of the ^{29}Si spectrum with Li insertion occurs only for SiCN-3 as shown in Fig. 3. This suggests that the mixed bond tetrahedra of Si also act as an additional Li storage site, although its role is estimated to be only minor based on the fact that the ^{7}Li spectra are almost identical for both SiCN-1 and SiCN-3 as shown in Fig. 2.

3.4. Temperature dependence of ^{7}Li spectra and spin-spin relaxation rate

Figure 5 shows the full width at half maximum (FWHM) $\Delta\nu$ and the spin-spin relaxation rate T_2^{-1} of ^{7}Li in lithiated SiCN samples as a function of temperature at two Larmor frequencies.

The FWHM increases rapidly with decreasing temperature and undergoes a crossover to a linear T behavior below $\sim$ 190 K. Also we find that the spin-spin relaxation rate T_2^{-1} follows the same T-dependence as the FWHM, as expected in the slow motion regime where $T_2^{-1} \propto \Delta\nu$. Although the FWHM and T_2^{-1} increase linearly below 190 K instead of reaching a plateau which would indicate the rigid lattice (RL) regime, it should be noted that the linear slope below 190 K for SiCN-3 is greatly reduced at a lower Larmor frequency of 33.1 MHz, while the data at $T > 190$ K are almost independent of frequency. Furthermore, we find that the slope for SiCN-1 and SiCN-3 at the same frequency of 116.64 MHz remains the same, as indicated by solid lines, despite their different T-dependence above 190 K. These results strongly suggest that the T-linear increase below 190 K could be an extrinsic effect being proportional to the external field strength. Therefore, we take 190 K as the onset temperature $T_{\rm onset}$ of the RL regime, above which the hopping diffusion of Li ions takes place leading to motional narrowing of the ^{7}Li linewidth.

In the high-temperature limit (i.e., motional narrowing limit), where the spin-spin relaxation rate is much smaller than the rigid-lattice linewidth i.e., $T_2^{-1} \ll \Delta\nu_{\mathrm{RL}}$, the NMR linewidth is independent of temperature and T_2^{-1} becomes proportional to the correlation time $\tau_c = \tau_0 \exp(E_A/k_B T)$. Thus, the temperature dependence of T_2^{-1} usually allows one to determine the activation energy E_A and τ_0 which are associated with the diffusive motion of Li ions. However, the motional narrowing limit is not accessible up to 420 K which is the highest temperature set by our equipment, as shown in Fig. 5. In this case, there is an alternative way to estimate E_A using the well-known empirical relation [15],

$$E_A \text{ (eV)} \sim 1.617 \times 10^{-3} T_{\mathrm{onset}} \text{ (K)}. \tag{2}$$

Using $T_{\mathrm{onset}} = 190$ K, one can obtain $E_A \sim 0.31$ eV (or ~ 3600 K) which indeed appears to be a reasonable value, being comparable to 0.32 eV for the fast 3D Li motion observed in another potential anode material [23] $Li_{12}Si_7$, and we will show below that the obtained E_A is consistent with temperature and frequency dependences of the spin-lattice relaxation rate measurements.

3.5. Lithium dynamics from the spin-lattice relaxation rates

Figure 6 shows the ^{7}Li spin-lattice relaxation rate T_1^{-1} as a function of temperature. T_1^{-1} continues to increase with increasing temperature up to 420 K, without forming a maximum which is expected when the condition $\omega_L \tau_c = 1$ is met from the Bloembergen, Purcell, and Pound (BPP) model [24],

$$T_1^{-1} \propto \frac{\tau_c}{1 + \omega_L^2 \tau_c^2}. \tag{3}$$

This indicates that the system lies in the low temperature limit, i.e. $\omega_L \tau_c \gg 1$, over the whole temperature range investigated.

Furthermore, we find that the Larmor frequency dependence of T_1^{-1} does not follow $T_1^{-1} \propto \omega_L^{-2}$ which is expected from the standard BPP model in Eq. (3), but obeys the relation $T_1^{-1} \propto \omega_L^{-3/2}$ instead. In general, such a non-BPP behavior could be attributed to both structural disorder and Coulomb interaction [25]. In particular, the 3/2 power law dependence of T_1^{-1} on ω_L is often observed in disordered materials and indicates that the Li ionic diffusion occurs continuously (continuum diffusion) due to varying atomic distances, rather than jump diffusion from one site to another [26, 15]. In this case, T_1^{-1} is expected to be proportional to $\tau_c^{-1/2}\omega_L^{n-2}$ with $n = 1/2$.

In addition to the ω_L-dependence, the data reveal the presence of a background T_1^{-1} which arises from contributions that are unrelated to the diffusion process, which is clearly revealed in the Arrhenius plot at low temperatures, as shown in Fig. 7. Assuming a T linear background term, one can write:

$$T_1^{-1} = a_0 \frac{1}{\sqrt{\tau_c}} \omega_L^{-3/2} + c_0 \omega_L^{-1/2} T, \tag{4}$$

where $\tau_c \equiv \tau_0 \exp(E_A/k_B T)$, and a_0 and c_0 are constants which are allowed to vary depending on the samples.

We find that this formula excellently describes the temperature and ω_L-dependence of the T_1^{-1} data for SiCN-3a, using $E_A = 0.31$ eV obtained above and $\tau_0 = 1.3$ ps. We constrained the parameters a_0 and c_0 to keep their values during the fit of the T_1^{-1} data at 33.1 and 116.64 MHz for SiCN-3a, in order to ensure the correct ω_L-dependence of T_1^{-1}. The fitted results are shown as solid lines in Figs. 6 and 7. For SiCN-1a and SiCN-3b, a_0 and c_0 are allowed to be slightly adjusted, but the E_A and τ_0 values obtained above still

hold. In fact, the T_1^{-1} of SiCN-1a is essentially the same as that of SiCN-3a with a small offset, as shown in Fig. 7. Note that the E_A corresponds to the activation energy in the high T regime, $E_A^{\rm HT}$, so that the effective activation energy $E_A/2$ from Eq. (4) is equivalent to $E_A^{\rm LT}$ in the low T regime that satisfies the relation $E_A^{\rm LT} = (1-n)E_A^{\rm HT}$ with $n = 1/2$ [27].

In order to get further information on the slow motion of Li ions, we measured the rotating frame relaxation rate, $T_{1\rho}^{-1}$, which is sensitive to slow motion in the kHz frequency scale. Since the T_1^{-1} measurements yielded the same diffusion parameters for both SiCN-1a and SiCN-3a samples, we carried out the $T_{1\rho}^{-1}$ measurements on the SiCN-3a sample only. We find that the relaxation of the nuclear magnetization $M_\rho(t)$ in the rotating frame is strongly stretched in its initial decay, in contrast to the T_1^{-1} experiments where the relaxation of $M(t)$ is always single exponential. This non-exponential decay of $M_\rho(t)$ along the rotating field is attributed to limited spin diffusion in which the direct relaxation rate is faster than the diffusion rate [28, 29]. In this case, one may expect that $M_\rho(t)$ decays exponentially at long times where the diffusion rate becomes important. Indeed, we observed a single exponential decay at long times. Here, we extracted $T_{1\rho}^{-1}$ in two ways, one from taking t when $M_\rho(t) = M_\rho(0)/e$ and the other from the fit of the exponential decay at long times, $T_{1\rho,s}^{-1}$ and $T_{1\rho,l}^{-1}$, respectively. $T_{1\rho,l}^{-1}$ as a function of T is shown in Fig. 6, exhibiting a clear characteristic temperature $T_{\rm max}$ at which the spin-lattice relaxation rates pass through a maximum. Remarkably, $T_{\rm max}$ is very close to 260 K at which $2\omega_1\tau_c = 1$, where ω_1 is the Larmor frequency in the RF field, with the same diffusion parameters E_A and τ_0 deduced above. This is another evidence that the correlation time τ_c describing the Li ionic

motion in SiCN is uniquely given by well-defined parameters.

In contrast to the long rate $T_{1\rho,l}^{-1}$, the short rate $T_{1\rho,s}^{-1}$ does not reveal a maximum as shown in Fig. 7 similar to the case of T_1^{-1}. This suggests that $T_{1\rho,s}^{-1}$ is largely caused by the mechanism related to the fast Li motion. Indeed, its behavior in terms of inverse temperature, particularly at low T, seems to be described by Eq. (4) with the same activation energy E_A used for the T_1^{-1} fit (green solid line in Fig. 7). Then, one may interpret that, on top of the usual activation behavior (denoted by the green solid line), the additional enhancement of $T_{1\rho,s}^{-1}$ with respect to the green line (see the down arrow in Fig. 7) at high temperatures is superimposed. This enhancement centered near 300 K may be related to the slow diffusive motion of Li.

While the $T_{1\rho,l}^{-1}$ data reveal $T_{\max}$ being consistent with the correlation time, the values of $T_{1\rho,l}^{-1}$ are too small compared to those of T_1^{-1}, as shown in Fig. 6. This unusual feature found in the $T_{1\rho,l}^{-1}$ data as well as the seeming coexistence of the two different mechanisms in the $T_{1\rho,s}^{-1}$ data may suggest that the slow motion of Li ions is given by a rather complex process compared to their fast motion which is well understood by the simple activation law.

Despite the complex rotating frame relaxation rates detected on a slow timescale, our NMR relaxation measurements show that the fast dynamics of Li on a timescale of μs, which is of practical importance for the performance of anode materials, is essentially described by a "single" activation energy and correlation time in a wide temperature range. This is a quite remarkable finding, taking into consideration that the structural disorder in amorphous materials like SiCN usually causes a distribution of either activation energy or correlation times or both.

4. Conclusions

We carried out systematic NMR studies focusing on the ^{7}Li spectra and relaxation rates as a function of temperature in the two SiCN ceramics derived from polysilylcarbodiimide (HN1) and polysilazane (HN3). Our study successfully characterized the *local* Li diffusion process in these materials by NMR linewidth and relaxation measurements. The dependence on Li insertion/extraction of the ^{29}Si and ^{13}C NMR spectra revealed that both sp^2 and sp^3 free carbons act as major electrochemically active sites for Li storage. The comparison between the ^{29}Si spectra of SiCN-1 and SiCN-3 show that an additional path for Li storage can be formed in SiCN-3 through the mixed bond tetrahedra of Si.

We found that the ^{7}Li line narrowing occurs at 190 K, which allows an estimation of the activation energy of 0.31 eV. Apart from the slow motion regime of Li which seems to be affected by complicated diffusion and/or non-diffusion processes, the temperature and Larmor frequency dependences of the ^{7}Li relaxation rates demonstrated that the Li dynamics in the polymer-derived SiCN ceramics in a wide operational temperature range from 200 to 400 K is governed by a very stable thermal activation law given by well-defined diffusion parameters. The stable diffusion mechanism of SiCN ceramics regarding temperature variation suggests that one may fine-tune the Li diffusion parameters for an anode material optimized for specific battery performance, without the need for the detailed understanding of the structural complexity in these amorphous materials.

Acknowledgement

We thank Yan Gao for her help in polymer synthesis. This research was financially supported by the DFG within the priority program SPP1473 (Grants No. GR3330/3-1 and GR 4440/1-2) and the collaborative research center SFB 595/A4.

References

[1] R. Riedel, G. Mera, R. Hauser, A. Klonczynski, Silicon-based polymer-derived ceramics: Synthesis properties and applications-a review, J. Ceram. Soc. Jpn. 114 (2006) 425–444. doi:10.2109/jcersj.114.425.

[2] P. Colombo, G. Mera, R. Riedel, G. D. Sorarù, Polymer-derived ceramics: 40 years of research and innovation in advanced ceramics, J. Am. Ceram. Soc. 93 (2010) 1805–1837. doi:10.1111/j.1551-2916.2010.03876.x.

[3] A. Wilson, G. Zank, K. Eguchi, W. Xing, J. Dahn, Pyrolysed silicon-containing polymers as high capacity anodes for lithium-ion batteries, J. Power Sources 68 (1997) 195 – 200. doi:10.1016/S0378-7753(96)02551-7.

[4] G. Ziegler, H.-J. Kleebe, G. Motz, H. Müller, S. Traßl, W. Weibelzahl, Synthesis, microstructure and properties of sicn ceramics prepared from tailored polymers, Mater. Chem. Phys. 61 (1999) 55 – 63. doi:http://dx.doi.org/10.1016/S0254-0584(99)00114-5.

[5] R. Kolb, C. Fasel, V. Liebau-Kunzmann, R. Riedel, Sicn/c-ceramic composite as anode material for lithium ion batteries, J. Eur. Ceram. Soc. 26 (2006) 3903 – 3908. doi:10.1016/j.jeurceramsoc.2006.01.009.

[6] Y. Feng, Electrochemical properties of heat-treated polymer-derived sicn anode for lithium ion batteries, Electrochim. Acta 55 (2010) 5860 – 5866. doi:10.1016/j.electacta.2010.05.036.

[7] G. Mera, A. Navrotsky, S. Sen, H.-J. Kleebe, R. Riedel, Polymer-derived sicn and sioc ceramics - structure and energetics at the nanoscale, J. Mater. Chem. A 1 (2013) 3826–3836. doi:10.1039/C2TA00727D.

[8] G. Liu, J. Kaspar, L. M. Reinold, M. Graczyk-Zajac, R. Riedel, Electrochemical performance of dvb-modified sioc and sicn polymer-derived negative electrodes for lithium-ion batteries, Electrochim. Acta 106 (2013) 101 – 108. doi:http://dx.doi.org/10.1016/j.electacta.2013.05.064.

[9] G. Mera, R. Riedel, F. Poli, K. Müller, Carbon-rich sicn ceramics derived from phenyl-containing poly(silylcarbodiimides), J. Eur. Ceram. Soc. 29 (2009) 2873 – 2883. doi:10.1016/j.jeurceramsoc.2009.03.026.

[10] M. Graczyk-Zajac, G. Mera, J. Kaspar, R. Riedel, Electrochemical studies of carbon-rich polymer-derived sicn ceramics as anode materials for lithium-ion batteries, J. Eur. Ceram. Soc. 30 (2010) 3235 – 3243. doi:10.1016/j.jeurceramsoc.2010.07.010.

[11] J. Kaspar, G. Mera, A. P. Nowak, M. Graczyk-Zajac, R. Riedel, Electrochemical study of lithium insertion into carbon-rich polymer-derived silicon carbonitride ceramics, Electrochim. Acta 56 (2010) 174 – 182. doi:10.1016/j.electacta.2010.08.103.

[12] N. Liao, W. Xue, M. Zhang, Effect of carbon content on structural and

mechanical properties of sicn by atomistic simulations, J. Eur. Ceram. Soc. 32 (2012) 1275 – 1281. doi:10.1016/j.jeurceramsoc.2011.11.022.

[13] S. Widgeon, G. Mera, Y. Gao, E. Stoyanov, S. Sen, A. Navrotsky, R. Riedel, Nanostructure and energetics of carbon-rich sicn ceramics derived from polysilylcarbodiimides: Role of the nanodomain interfaces, Chem. Mater. 24 (2012) 1181–1191. doi:10.1021/cm2038238.

[14] C. P. Grey, N. Dupré, Nmr studies of cathode materials for lithium-ion rechargeable batteries, Chem. Rev. 104 (2004) 4493–4512. doi:10.1021/cr020734p.

[15] P. Heitjans, A. Schirmer, S. Indris, Diffusion in Condensed Matter: Methods, Materials, Models, Springer, 2005, Ch. NMR and β-NMR Studies of Diffusion in Interface-Dominated and Disordered Solids.

[16] R. Böhmer, K. Jeffrey, M. Vogel, Solid-state li nmr with applications to the translational dynamics in ion conductors, Prog. Nucl. Magn. Reson. Spectrosc. 50 (2007) 87 – 174. doi:10.1016/j.pnmrs.2006.12.001.

[17] Y. Iwamoto, W. Völger, E. Kroke, R. Riedel, T. Saitou, K. Matsunaga, Crystallization behavior of amorphous silicon carbonitride ceramics derived from organometallic precursors, J. Am. Ceram. Soc. 84 (2001) 2170–2178. doi:10.1111/j.1151-2916.2001.tb00983.x.

[18] H. Fukui, H. Ohsuka, T. Hino, K. Kanamura, A si-o-c composite anode: High capability and proposed mechanism of lithium storage associated with microstructural characteristics, ACS Appl. Mater. Interfaces 2 (2010) 998–1008. doi:10.1021/am100030f.

[19] H. Fukui, H. Ohsuka, T. Hino, K. Kanamura, Influence of polystyrene/phenyl substituents in precursors on microstructures of si-o-c composite anodes for lithium-ion batteries, J. Power Sources 196 (2011) 371 – 378. doi:10.1016/j.jpowsour.2010.06.077.

[20] L. M. Reinold, M. Graczyk-Zajac, Y. Gao, G. Mera, R. Riedel, Carbon-rich sicn ceramics as high capacity/high stability anode material for lithium-ion batteries, J. Power Sources 236 (2013) 224 – 229. doi:10.1016/j.jpowsour.2013.02.046.

[21] D. Ahn, R. Raj, Cyclic stability and c-rate performance of amorphous silicon and carbon based anodes for electrochemical storage of lithium, J. Power Sources 196 (2011) 2179 – 2186. doi:10.1016/j.jpowsour.2010.09.086.

[22] J. Bill, J. Seitz, G. Thurn, J. Dürr, J. Canel, B. Z. Janos, A. Jalowiecki, D. Sauter, S. Schempp, H. P. Lamparter, J. Mayer, F. Aldinger, F.Aldinger, Structure analysis and properties of si-c-n ceramics derived from polysilazanes, phys. stat. sol. (a) 166 (1998) 269–296. doi:10.1002/(SICI)1521-396X(199803)166:1<269::AID-PSSA269>3.0.CO;2-7.

[23] A. Kuhn, P. Sreeraj, R. Pöttgen, H.-D. Wiemhöfer, M. Wilkening, P. Heitjans, Li ion diffusion in the anode material Li12Si7: Ultrafast quasi-1d diffusion and two distinct fast 3d jump processes separately revealed by 7li nmr relaxometry, J. Am. Chem. Soc. 133 (2011) 11018–11021. doi:10.1021/ja2020108.

[24] N. Bloembergen, E. M. Purcell, R. V. Pound, Relaxation effects in nuclear magnetic resonance absorption, Phys. Rev. 73 (1948) 679–712. doi:10.1103/PhysRev.73.679.

[25] M. Meyer, P. Maass, A. Bunde, Spin-lattice relaxation: Non-bloembergen-purcell-pound behavior by structural disorder and coulomb interactions, Phys. Rev. Lett. 71 (1993) 573–576. doi:10.1103/PhysRevLett.71.573.

[26] J. L. Bjorkstam, M. Villa, Second-order quadrupolar and low-dimensionality effects upon nmr resonance spectra, Phys. Rev. B 22 (1980) 5025–5032. doi:10.1103/PhysRevB.22.5025.

[27] K. Ngai, O. Kanert, Comparisons between the coupling model predictions, monte carlo simulations and some recent experimental data of conductivity relaxations in glassy ionics, Solid State Ionics 53-56 (1992) 936. doi:10.1016/0167-2738(92)90275-T.

[28] D. Tse, I. J. Lowe, Nuclear spin-lattice relaxation in caf2 crystals via paramagnetic centers, Phys. Rev. 166 (1968) 292–302. doi:10.1103/PhysRev.166.292.

[29] G. Balzer-Jöllenbeck, O. Kanert, H. Jain, K. L. Ngai, New interpretation of activation enthalpies for electrical conductivity and nuclear spin relaxation in glassy ionic conductors, Phys. Rev. B 39 (1989) 6071–6075. doi:10.1103/PhysRevB.39.6071.

Table 1: Elemental composition of SiCN-1 and SiCN-3 in wt%. The calculation of the free carbon content [wt%] was done by neglecting the amount of chlorine and hydrogen in the samples.

Sample	Si	C	N	O	H	Cl	Free C	Empirical formula
SiCN-1	28.70	54.94	14.73	0.96	0.60	0.05	52.7	$Si_1C_{4.47}N_{1.03}O_{0.06}H_{0.58}$
SiCN-3	34.41	47.71	13.28	0.87	0.27	3.46	43.3	$Si_1C_{3.24}N_{0.77}O_{0.04}H_{0.22}Cl_{0.08}$

Table 2: Lithiation/delithiation capacities (C_{li}/C_{deli}) and coulombic efficiency (η) for investigated samples.

Sample	C_{li} [mAh·g^{-1}]	C_{deli} [mAh·g^{-1}]	η [%]
SiCN-1a	552	-	-
SiCN-1b	404	218	54
SiCN-3a	492	-	-
SiCN-3b	416	251	60

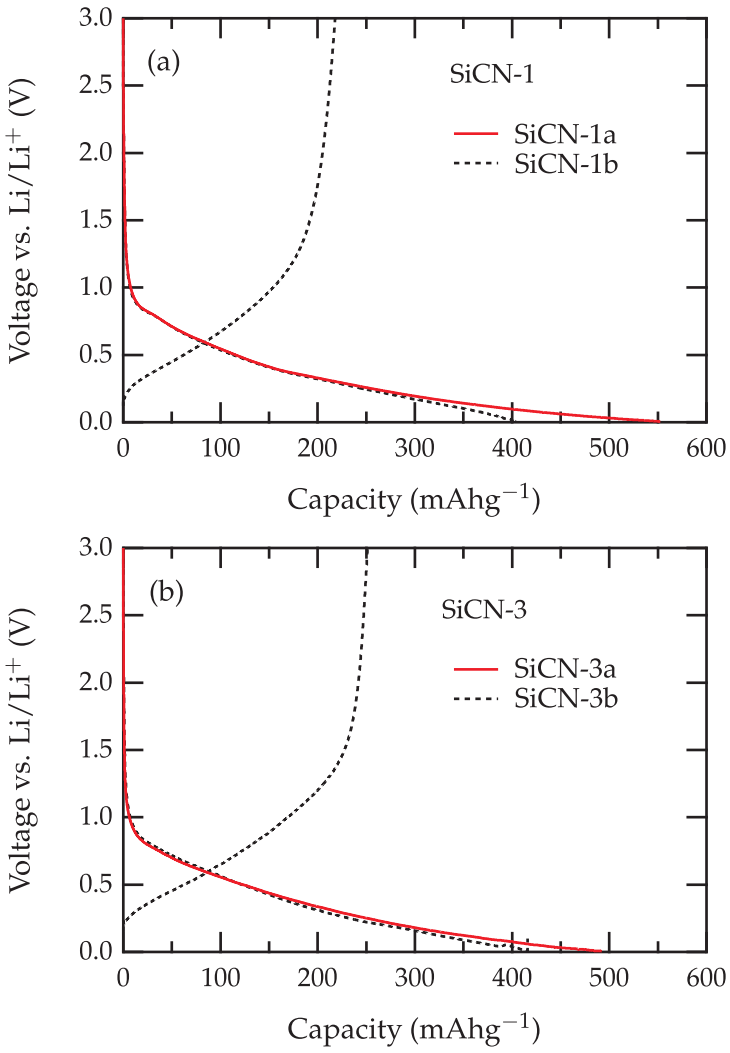

Figure 1: Voltage vs. Li/Li^+ over capacity curves of the investigated samples. Lithiation curves of SiCN-1a and SiCN-3a are given by continuous red lines. The dashed black lines display lithiation and delithiation curves of SiCN-1b and SiCN-3b, respectively.

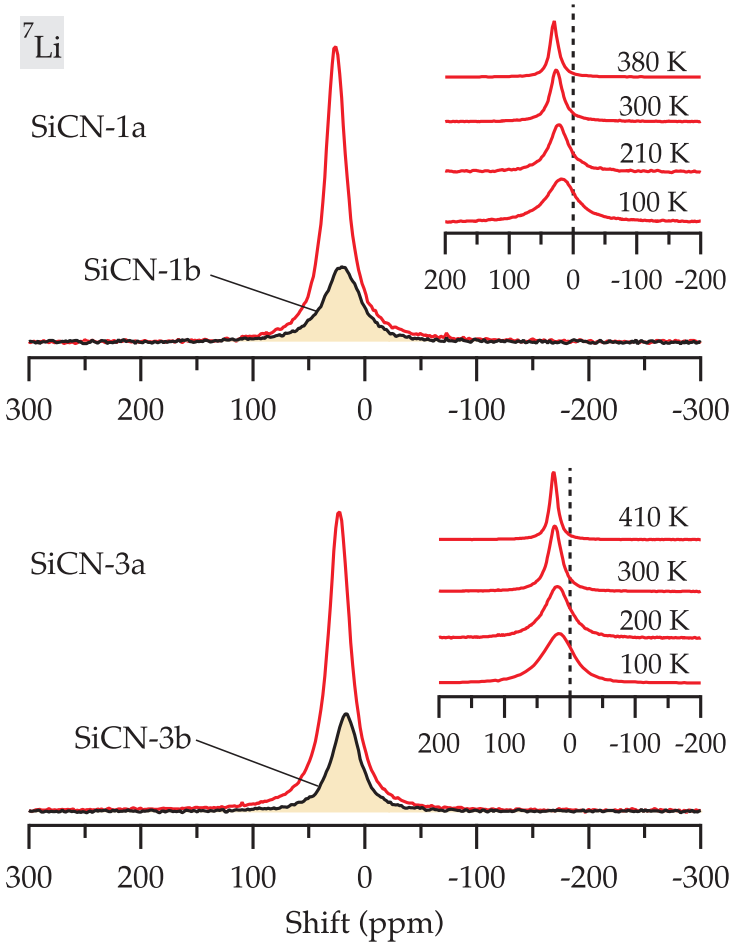

Figure 2: ^{7}Li NMR spectra of SiCN-1a and SiCN-3a samples taken at 300 K at 116.64 MHz. The ^{7}Li spectra measured after Li extraction are compared. Clearly, the spectral weight at larger shift is significantly depleted after discharging. The ^{7}Li spectra at chosen temperatures are shown in the inset.

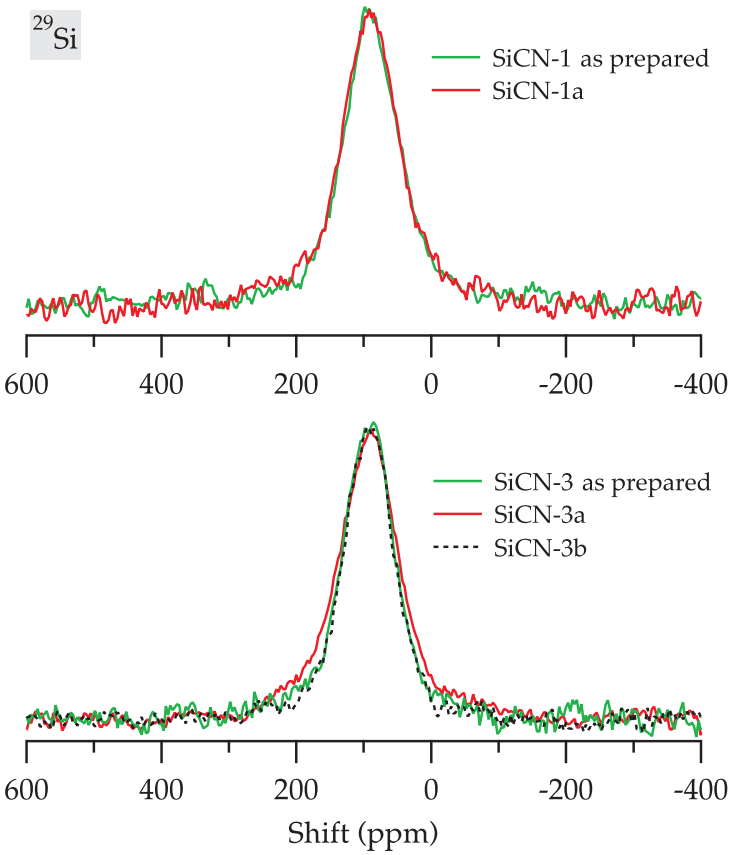

Figure 3: ^{29}Si NMR spectra of SiCN-1 and SiCN-3 samples obtained at 300 K at 59.624 MHz. While Li insertion/extraction has little influence on the spectrum for SiCN-1, a small broadening was identified after Li insertion for SiCN-3. Note that the broadening effect disappears after Li extraction.

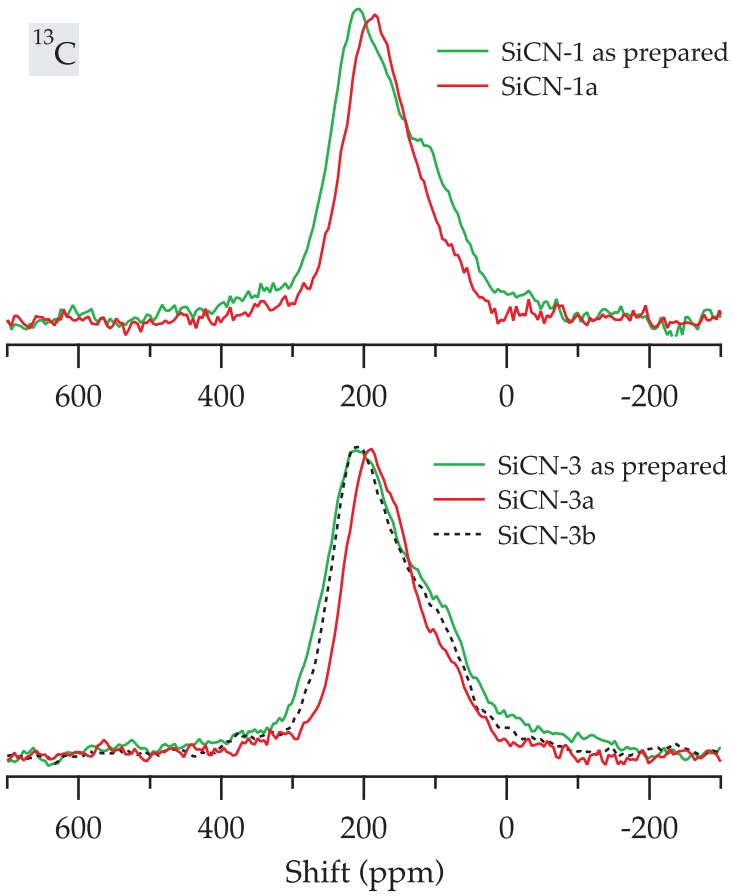

Figure 4: ^{13}C NMR spectra of SiCN-1 and SiCN-3 samples measured at 300 K and 75.476 MHz. Li insertion has a significant influence on the ^{13}C for both SiCN-1 and SiCN-3 in contrast to ^{29}Si, indicating that Li ions mostly reside near carbon sites regardless of the detailed local structure.

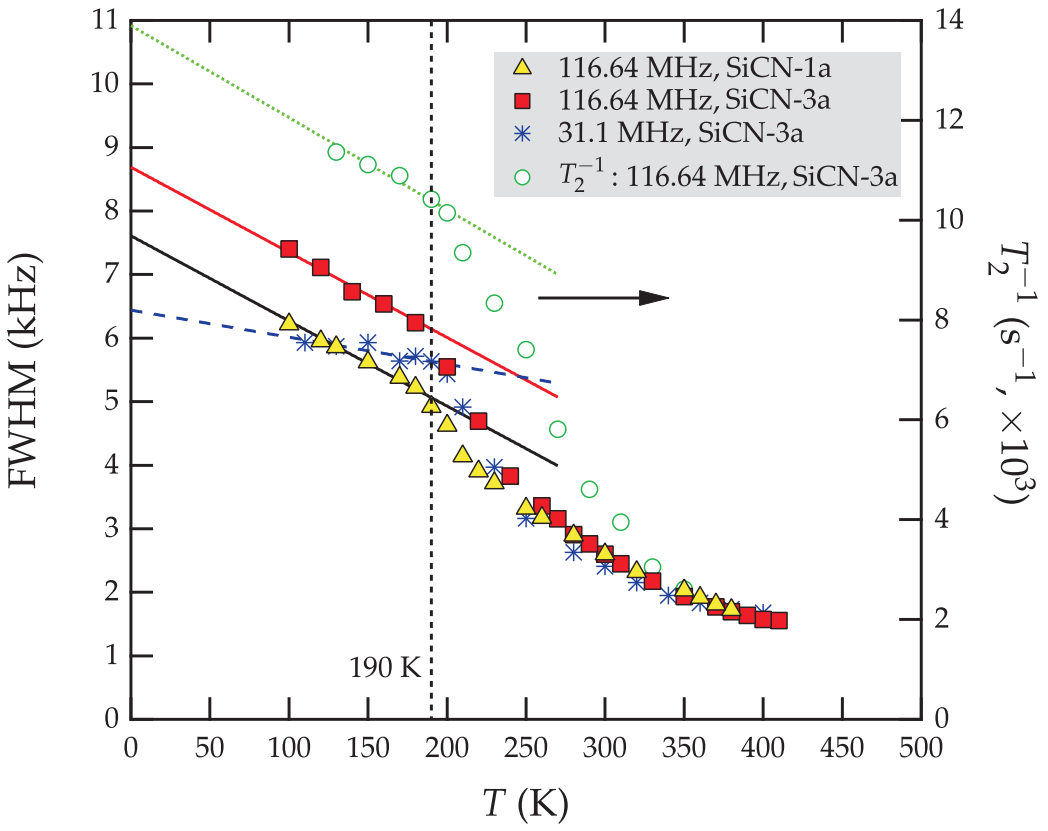

Figure 5: Temperature dependence of the ^{7}Li NMR linewidth and spin-spin relaxation rate T_2^{-1}. The data increase rapidly with decreasing temperature and a crossover to a T-linear behavior below $\sim$ 190 K occurs, regardless of Larmor frequencies for both SiCN-1 and SiCN-3 ceramics.

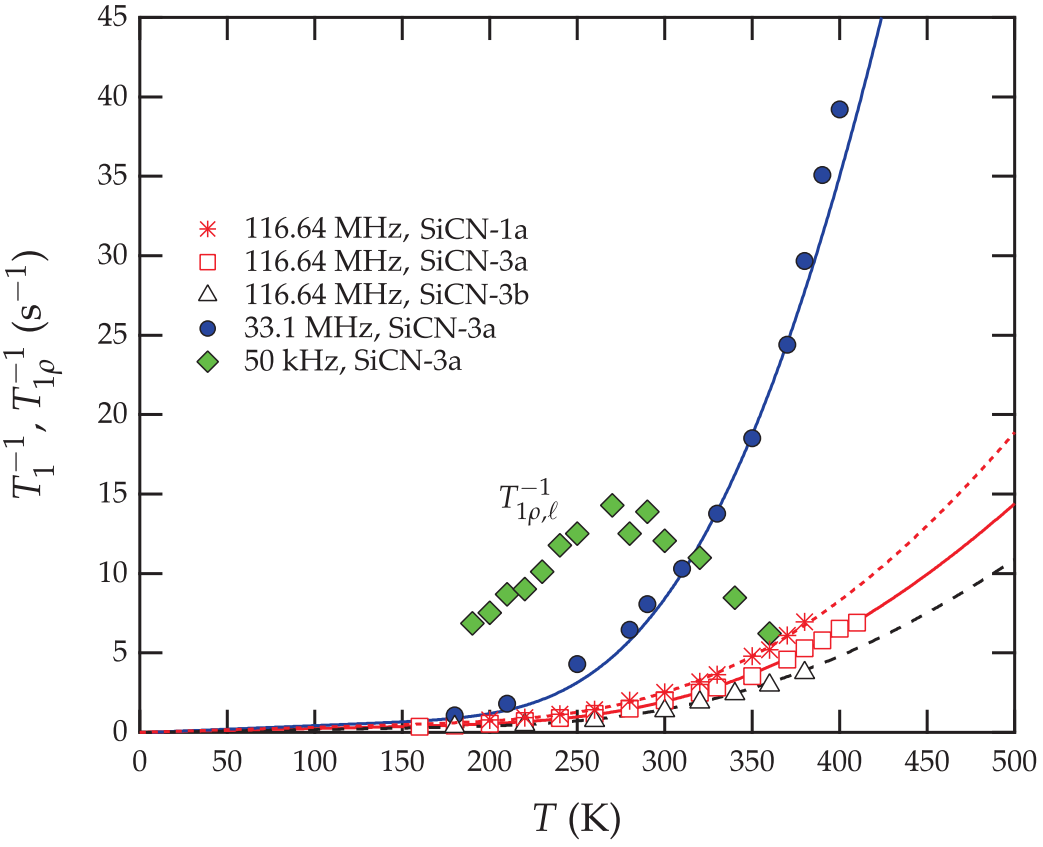

Figure 6: Temperature dependence of the ^{7}Li spin-lattice relaxation rates T_1^{-1} in the laboratory frame and $T_{1\rho}^{-1}$ in the rotating frame. $T_{1\rho}^{-1}$ (green diamond symbol) was measured at 50 kHz on the SiCN-3a sample. The theoretical fits to the data are from Eq. 4 with $E_A = 3600$ K and $\tau_0 = 1.3$ ps, demonstrating the $\omega_L^{-3/2}$ dependence of T_1^{-1}.

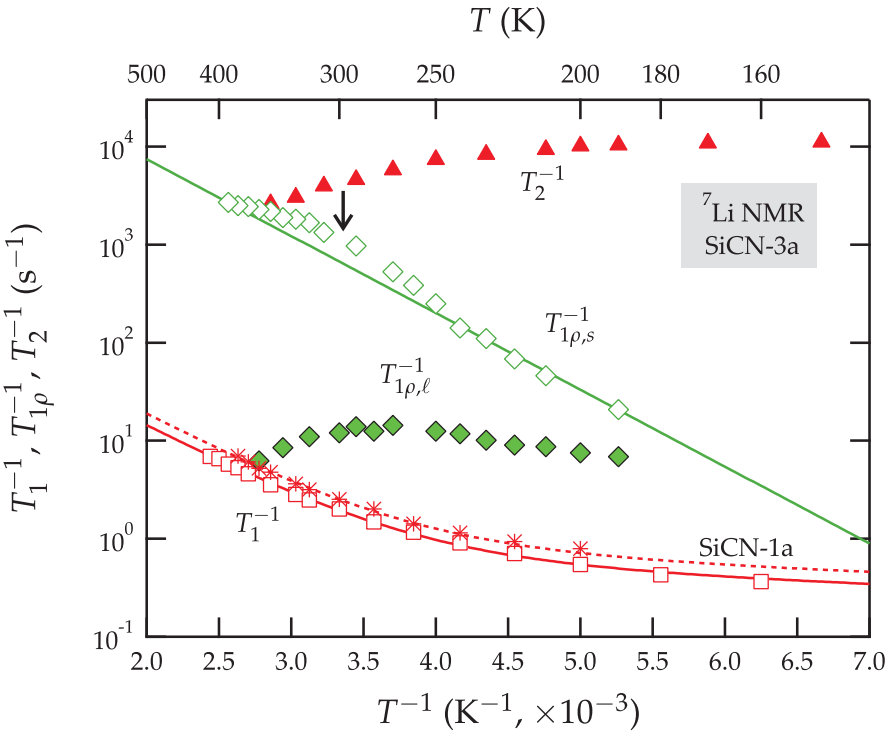

Figure 7: Comparison of ^{7}Li relaxation rates T_1^{-1} and T_2^{-1} at 116.64 MHz and $T_{1\rho}^{-1}$ at 50 kHz as a function of inverse temperature measured in SiCN-3a. T_1^{-1} of SiCN-1a at 116.64 MHz (red asterisks with dashed line) is almost identical to that of SiCN-3a. For both samples, a T-linear background at low temperatures superimposed on the diffusion-related activation behavior is clearly visible in T_1^{-1}.